SCIENTIFIC COMMITTEE
SIXTEENTH REGULAR SESSION

ELECTRONIC MEETING
11-20 August 2020

Developing yellowfin tuna recruitment indices from drifting FAD purse seine catch and effort data

WCPFC-SC16-2020/SA-IP-08

Tiffany Vidal[1] and Paul Hamer[1]

[1] 1Oceanic Fisheries Programme (OFP), The Pacific Community, Nouméa, New Caledonia

Contents

Executive Summary

The assessment of yellowfin tuna *Thunnus albacares* from the western and central Pacific Ocean (WCPO) relies heavily on fishery-dependent data to inform the assessment model on trends in biomass. The longline fishery, which primarily targets adult yellowfin provides key inputs to the assessment; however these data may be unreliable when it comes to monitoring trends in the juvenile component of the population. Estimation of recruitment to the fishery (approximately age-1 yellowfin) represents an important uncertainty in the assessment of yellowfin because recruitment deviations may confound the biomass scaling parameter. The assessment model is configured in a way that enables recruitment estimates to be adjusted to explain changes in the catch that may not be accounted for by the trend in a CPUE index. As a result, there may be limited biological inference to be made from these trends, and the resulting estimates may be influenced by other data inputs, potentially unrelated to trends in recruitment. To more explicitly inform the 2020 stock assessment model on trends in yellowfin recruitment dynamics, we have explored the use of operational catch and effort data from purse seine sets made on drifting fish aggregating devices (dFADs) to develop relative recruitment indices. This paper summarizes the characteristics of the dFAD fishery, data preparation, and modeling approach to develop a recruitment index from purse seine fishery catch and effort data.

Using operational (set-level) purse seine catch and effort data reported by the Pacific Islands Regional Fisheries Observer Program from 2010-2018, we employed a suite of spatiotemporal delta-Gamma models to implicitly account for variability in space and time and to explicitly control for variables predicted to influence catchability of yellowfin tuna. There was little variability among the models with respect to the resulting regional abundance indices. The preferred model structure included vessel length, species composition cluster variable, and set time (modeled as hours before sunrise) as catchability covariates, and a spatially-varying effect of the El Niño Southern Oscillation index as a habitat covariate expected to influence local density. The abundance indices were relatively stable over the time period evaluated, with a notable disconnect between the recruitment indices estimated from the most recent (2017) yellowfin stock assessment.

It should be noted that we have conducted this analysis to address an important data gap associated with yellowfin recruitment dynamics by using drifting FAD sets only as they are primarily associated with juvenile yellowfin harvest. However, adult fish were not excluded from the analysis, and therefore, we would not expect a direct link between the assessment estimates and the CPUE indices presented here. The abundance indices generated through this analysis would inform the assessment model, but would be evaluated with additional information on size composition and drifting FAD purse seine fishery selectivity. Together, with the additional assessment data inputs, the assessment model may be better able to estimate reliable abundance trends in the juvenile component of the yellowfin stock.

Given the prominence of the purse seine fleet in tuna removals throughout the WCPO, using catch and effort data from the fishery to inform the stock assessment, is a priority. There are however, important considerations associated with effort creep and associated time series

hyperstability that need additional attention. These concerns should not necessarily preclude these data, as valuable information may be gleaned from them; however, continued research into effort creep, fisher decision-making, changes in fishing strategies over time, and the development of a 'dashboard' of ancillary information from which to more reliably infer trends in tuna abundance is warranted.

We invite WCPFC-SC16 to note the results of this analysis and recommendations for future research:

Results

- Note the progress being made to standardize purse seine CPUE to better inform the stock assessment models on yellowfin recruitment trends.
- Note that over the shorter-term (2010-2018) yellowfin tuna abundance trends from drifting FAD sets appear to be relatively stable; however, when compared to longer-term logbook indices, the model suggests that abundance has declined over the past two decades.

Recommendations

- Recognize the importance of continued research to better understand the role of effort creep, including FAD-related technologies, on purse seine catch rates, and to support directed research to better understand technological creep and changes in fishing strategies through time, which may influence our understanding of effective effort through time.
- Conduct interviews with the purse seine industry, specifically with skippers and fishing masters, to better understand technological and strategic changes over time and inform analyses related to effort creep.
- Support additional biological data collection and analyses to improve our understanding of changes in age, growth, and recruitment dynamics in yellowfin, over time.
- Explore the potential for developing recruitment proxies from the extensive diet data available from the WCPO, through previous work done by the Pacific Community and research partners.
- Incorporate multiple data sources to further validate the signals detected from the CPUE analysis. For example, matching cohorts from longline and purse seine catches (using length frequency data) and further exploring correlation between the two as well as their relationships with CPUE and variability in the environment.

1 Background information

Yellowfin tuna *Thunnus albacares* is an important component of global fishery removals, and comprises approximately 25% of the tuna harvest from the western and central Pacific Ocean (WCPO) (Williams and Reid, 2019). Although the current status of the WCPO yellowfin stock suggests that it is not overfished, and that overfishing is not taking place, the overall biomass has declined through time, trending towards the overfished and overfishing reference points (Tremblay-Boyer et al., 2017). Relative abundance trends derived from longline catch and effort data serve as an important input to the yellowfin stock assessment models; however, the longline fishery primarily targets adult yellowfin, and as a result the index of relative abundance from this fishery may not provide an accurate representation of dynamics in the juvenile component of the population. Developing a recruitment index from juvenile catch rates may help to address uncertainty in recruitment strength, improve model fit, and reduce bias. In 2017, the assessment results suggested that recruitment had generally declined through time (since the 1950s); however, in recent years (2011-2015), there was a slight increase in recruitment strength. Due to a paucity of information, recruitment represented an important source of uncertainty in the assessment model (Tremblay-Boyer et al., 2017) because the model can use recruitment to compensate for changes in catch that cannot be accounted for by the trend in a CPUE index.

To address this uncertainty, we are exploring the potential for catch and effort information from purse seine sets made on drifting fish aggregating devices (dFADs) to be used to inform the assessment model regarding recent trends in recruitment. Here, recruitment is defined as recruitment of juveniles to the fishery (i.e. approximately age-1 yellowfin).

The purse seine fishery accounts for approximately 56% of the yellowfin removals from the Western and Central Pacific Convention Area (WCP-CA) (Williams and Reid, 2019), and is largely harvested using two main fishing strategies: setting on FADs (i.e. associated sets) or setting on free schooling tunas, unassociated with floating objects (i.e. unassociated sets). It has been shown that free-school sets are typically composed of adult yellowfin and larger skipjack, whereas FAD sets are more apt to catch smaller skipjack along with juvenile yellowfin and bigeye (Williams and Reid, 2019). We have attempted to leverage information collected by fisheries observers on the catch rates from dFAD sets to shed light on recruitment dynamics of yellowfin tuna.

2 Methods

The development of a recruitment index, in this context, is analogous to a traditional standardization of fishery-dependent CPUE for use as an abundance index. Nominal CPUE is standardized, to remove the effect of factors that influence catch rates, other than changes in abundance over time. Such factors are typically related to catchability, and can reflect differential efficiency or skill measures (e.g. vessel size, skipper experience), and require 'standardization' to reveal the underlying trend in population dynamics. In this analysis, we are standardizing CPUE from dFAD sets only, because yellowfin harvested from these sets are predominantly associated

with juvenile size classes. The standardized index, estimated from the model, represents an area-weighted abundance; however, such indices are most informative with respect to relative trends, as the catch data will inform the overall biomass scaling. Therefore, to be able to compare relative trends among models to the nominal CPUE, we standardize the indices to the mean, therefore, all indices have a mean of one and can be compared directly. It should be noted, that although larger, adult yellowfin are also harvested in dFAD sets, the recruitment (juvenile) index developed here will be assessed, within the stock assessment model, in conjunction with size-composition data and gear-specific selectivities, thereby disentangling of the juvenile signal.

2.1 Data description and preparation

The yellowfin stock assessment spatial domain, extends roughly from 50°N to 40°S and from 110°E to 170°W; however, the purse seine sector of the yellowfin fishery primarily operates within the 2017 stock assessment regions 3, 4, and 8 (Tremblay-Boyer et al., 2017; Figure 1), and therefore, we narrowed the focus of this analysis to those regions only. Operational (set-level) purse seine CPUE (mt/set) data were obtained from the Pacific Islands Regional Fisheries Observer Program data for the tuna purse seine fleets operating within the western and central Pacific Ocean (WCPO). As of 2010, 100% of tuna purse seine trips in the region were required to carry a fisheries observer; therefore, to take advantage of the additional confidence in data quality observer coverage provides, we used a time series which extended from 2010 through 2018 for this analysis.

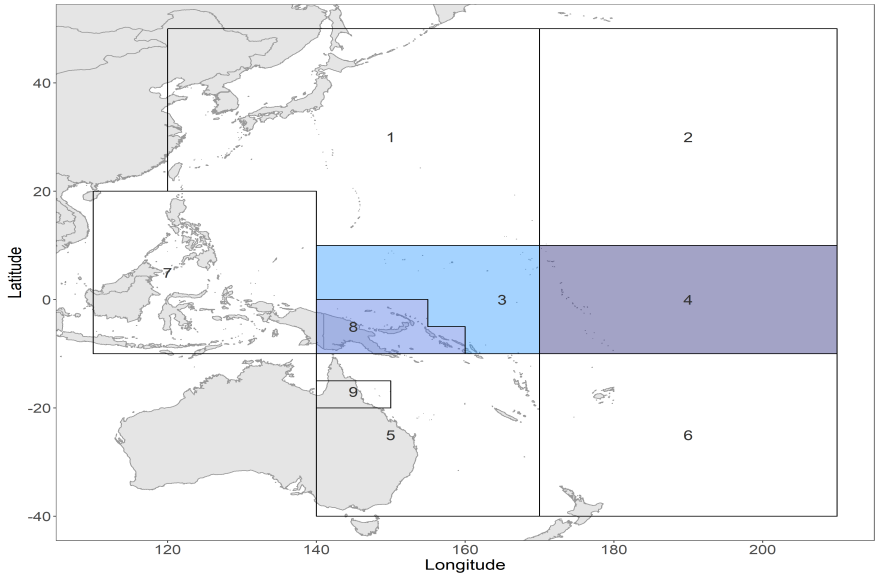

Figure 1: Regional structure used in the 2017 stock assessment. The dominant regions of purse seine activity and the focus for this paper, are shaded in blue.

The focus of this analysis is juvenile yellowfin (i.e. approximately age 1); these are primarily harvested from purse seine sets made around dFADs, whereas unassociated sets tend to harvest larger, adult yellowfin (Figure 2). Given our focus on producing an index of recruitment, we

analyzed data from dFAD sets only. The full data set (n= 79,384) was filtered to only include vessels between 50 and 80 m in length that were active in the fishery for approximately 20% of the time series of interest, excluding the quarters associated with the FAD closure periods (i.e. observed fishing activity in at least 5 quarters between 2010 and 2018). In addition, any vessel that entered the fishery in 2017 or later, was retained for the analysis. The vessel size criterion was imposed due to the implementation of the Vessel Day Scheme (VDS) in 2008. The VDS is an effort-based management framework, which applied a fishing day differential based on vessel length (Dunn et al., 2006; Parties to the Nauru Agreement, 2016). Vessels within the 50-80 m range are charged one vessel day for one fishing day, while larger vessels are charged 1.5 vessel days per calendar day of fishing, and smaller vessels 0.5 days. Over the past decade, many of the largest vessels have left the fishery, leaving a fleet that is dominated by the 50-80 m size class (Figure 5); thus, focusing on this vessel size class will help ensure the indicator is robust to future changes in industry structure.

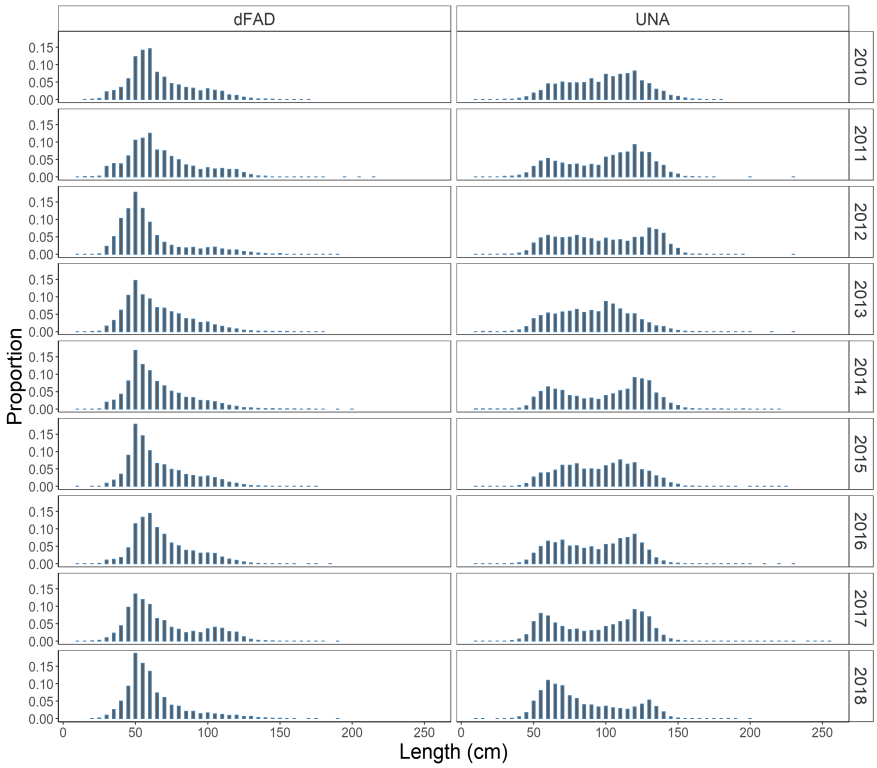

Figure 2: Distribution of yellowfin length frequencies (fork length), collected by observers, for drifting FAD (dFAD) and free school (UNA) purse seine sets from 2010-2018.

In the interest of analyzing catch and effort that is representative of the fishery, we omitted sets with less then one metric tonne (mt) of total tuna catch, as these were assumed to be failed sets. A failed set is different from a skunk set, in that a purse seiner is unlikely to set on a very small school (typically $<$ 10 mt, but rarely on a school $<$3-5 mt). Therefore, a catch of $<$1 mt was assumed to represent a failure in the fishing operation which led to an unusually small catch. Extreme outlier catch values ($>$ 99th quantile of catches), sets made within the three-month FAD

closure period, and observations with missing data, were removed from the data prior to analysis. Lastly, sets made outside a five hour window around sunrise were excluded, as the validity of the set times were questionable. This potentially excludes sets made later in the day; however, we felt this was a conservative approach to focus the analysis on the main efforts of the fishery. The filtered data set consisted of 38,740 observations (Table 1).

Filtering criteria	Removal %	Removal #
Vessel participation (>20% of time series; ~5 quarters)	12%	9,320
Vessels between 50 and 80 m	16%	13,033
Removal of failed sets (total tuna catch) < 1 mt	1%	853
Extreme catch outliers (>99th quantile)	1%	562
Retained sets within 5 hours of sunrise	1%	774
Removed observations from the FAD closure period	3%	2,280
Remove records with missing data	17%	13,822

Table 1: Summary of data filtering criteria employed. Note that some observations would have been excluded based on multiple selection criteria; the numbers removed are based on sequential filtering, and therefore may be an underestimate of observations relating to each criteria.

2.1.1 Covariates

Standardization of CPUE is aimed at removing the effect of variables that influence catchability while simultaneously accounting for factors which may influence local density. Traditional approaches to CPUE standardization, e.g. generalized linear modeling frameworks, treat all covariates as affecting catchability; whereas in the geostatistical modeling framework we have used for this analysis, a distinction is made between covariates that influence density and those that influence catchability (Thorson et al., 2015a; Thorson, 2019b). The model controls for the effects of the catchability covariates on the index by filtering them out, whereas the estimates are conditioned upon the density covariates (Thorson, 2019b). However, the distinction between which variables influence density and which influence catchability is not always straightforward.

We developed a suite of potential covariates predicted to influence yellowfin tuna catchability, for evaluation within the modeling framework. These factors were selected to capture vessel, gear, and fishing strategy characteristics (Table 2) as well as variability in the environment which may influence catch rates. Vessel and gear-based characteristics such as vessel length, net size, skiff horsepower, and well capacity, have generally increased through time (Vidal et al., 2020b) and were predicted to increase fishing efficiency over time. In addition, we included a species composition variable, based on a k-means clustering algorithm on proportion of the three main tuna species (yellowfin, skipjack *Katsuwonus pelamis*, and bigeye *Thunnus obesus*) in the catch. We used two clusters, largely to distinguish between sets dominated by skipjack and those dominated by yellowfin, as the school composition was predicted to be important in explaining variation in catch rates. Set time was considered a potentially important predictor variable because tuna tend to aggregate near the surface during the night and into the early morning hours before descending

to deeper waters to feed during the day. Typically, FAD sets are made prior to dawn (Harley et al., 2009), but in recent years purse seine vessels have occasionally been observed making multiple FAD sets in a single day; however, the practice remains rare. Following on previous work, we used hours before sunrise to represent set time, and modeled it as a catchability covariate. Time of sunrise (converted to UTC) was obtained using the *suncalc* R package (Agafonkin and Thieurmel, 2017), and was subtracted from the set time (reported in UTC). Positive values therefore, indicate a set was made after sunrise. Observations with set times extending beyond +/- 5 hours from sunrise were excluded from the analysis, due to concerns about misreported set times.

Variable	Description
Catchability covariates	
Year-quarter	Categorical: temporal variable related to inter-annual changes in abundance
Vessel length (m)	Continuous: overall vessel length (m)
Species composition cluster	Categorical: Indicates whether the catch is dominated by skipjack or yellowfin
Set time	Continuous: set time relative to sunrise (negative values are pre-dawn, positive, post-dawn)
Lunar phase	Categorical: new moon, first quarter, full, last quarter
Thermocline depth (m)	Continuous: estimated depth of the thermocline from the Global Ocean Data Assimilation System
Density covariates	
El Niño Southern Oscillation	Continuous: ENSO anomaly from Niño Region 4 (5N-5S, 160E-150W)
Sea surface temperature (C)	Continuous: predicted sea surface temperature from NOAA Optimal Interpolation, using high resolution data

Table 2: Description of catchability and density covariates evaluated in the model selection process.

The importance of oceanographic variables on catch rates of pelagic fishes has been well documented (e.g. Howell and Kobayashi, 2006; Bigelow and Maunder, 2007; Langley et al., 2009; Young et al., 2011). Within in this modeling framework, we have the flexibility to include habitat covariates predicted to influence yellowfin density and also catchability covariates predicted to influence capture vulnerability; variables that are controlled for when predicting density. Tuna habitat preference may be influenced by temperature, oxygen levels, and salinity (Arrizabalaga et al., 2015), as well as the density and distribution of prey fields; and therefore, capturing this variability in the environment may be informative for the models. Sea surface height has also been identified as a potentially important predictor of tuna density (Royer et al., 2004). Sea surface height anomalies can be altered by convergent and divergent areas (e.g. gyres), resulting in frontal zones which may attract aggregations of tunas due to enhanced prey availability (Lumban-Gaol et al., 2015). The El Niño Southern Oscillation (ENSO) was predicted to capture broader oceanographic features and variability in catch rates associated with the convergence zone in the western Pacific where the westward advection of cold, saline waters meet with an eastward advection of warm, low saline waters, creating an important frontal zone which promotes the

aggregation of plankton and micronekton as well as larger predators, such as tunas (Fiedler and Bernard, 1987; Lehodey et al., 1997). As this convergence zone shifts through time, the distribution and local density of tunas is predicted to shift as well. Lastly, lunar phase was considered as it has proven informative for explaining variability in catch rates of other pelagic fishes (e.g. Bigelow et al., 1999; Lowry et al., 2007; Evans et al., 2008). Bigeye tuna has been observed occupying deeper nighttime depths during the full moon as opposed to lesser illuminated phases (Evans et al., 2008). If yellowfin behave in a similar manner, this temporal vertical behavior could affect the proportion of fish vulnerable to purse seine gear throughout the lunar cycle. We obtained moon phase data using the R package *suncalc*, and categorized the phases into four categories: new moon, first quarter, full, and last quarter. Table 3 details the full list of oceanographic metrics we considered.

Metric	Description
sst	Sea surface temperature (C)
mean.sst	Mean sea surface temperature (C) in the upper 200 m of the water column
var.temp	Variance of sea surface temperature (C) in the upper 200 m of the water column
therm.depth	Depth (m) of the estimated thermocline
depth.20	Depth (m) of the 20° isotherm
sea.height	Estimated sea surface height (m)
mean.sal	Mean salinity in upper 200 m of the water column
var.sal	Variance of the salinity estimates for the upper 200 m of the water column
ENSO	ENSO anomaly index from Niño Region 4 (5N-5S, 160E-150W)

Table 3: Oceanographic metrics evaluated for use in the suite of standardization models.

We acknowledge that throughout the region of interest for this analysis, oceanographic variability is likely to be less important than in the more temperate waters. Oceanographic data for this analysis were obtained from several sources. Thermocline depth and depth of the 20° isotherm were calculated from the Global Ocean Data Assimilation System (GODAS), which is available monthly at a spatial resolution of 0.333° latitude by 1° longitude; high-resolution sea surface temperature data, aggregated to the day at a 0.25° degree spatial resolution, were obtained from the National Oceanic and Atmospheric Administration (Banzon et al., 2019); and salinity at depth data and sea surface height data were obtained from the E.U.s Copernicus Marine Service, available monthly at 1/12° spatial resolution.

2.2 Data summaries

The filtered data set has been summarized to illustrate the spatiotemporal distribution of catch and effort (Figures A.1 and 3). Variable correlations for vessel characteristics as well as oceanography metrics were evaluated to avoid problems of multicollinearity and to select a small

number of variables predicted to represent important sources of variability in the catch and effort data (Figure 4).

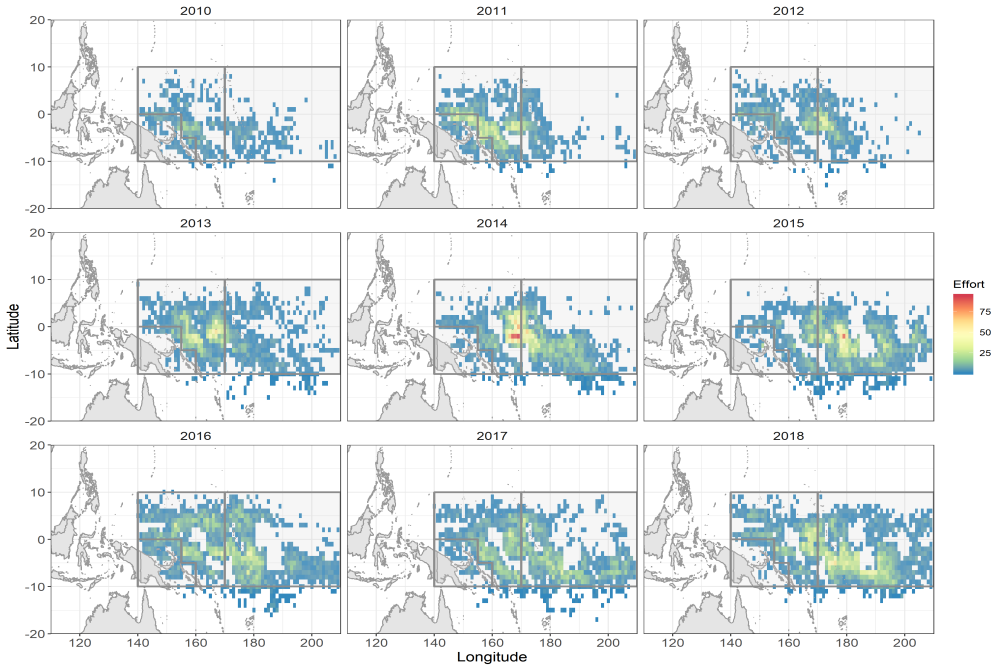

Figure 3: Distribution of dFAD sets from the filtered data set, by year, from 2010-2018.

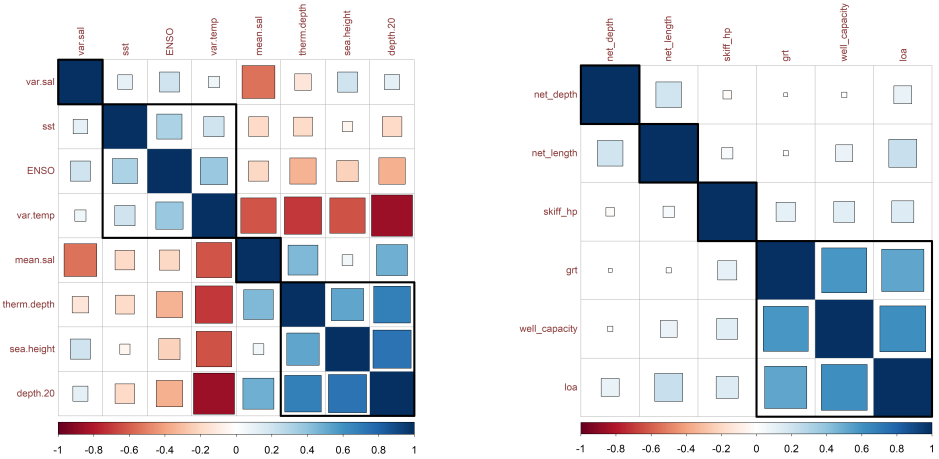

Figure 4: Hierarchical cluster correlation plots of the oceanographic and vessel characteristics variables considered for inclusion as catchability and density covariates in the suite of candidate models.

The correlation structure among the vessel-based characteristics suggested that gross registered tonnage, vessel length, and well capacity were highly correlated, with a moderate positive

correlation with skiff horsepower. Net length and net depth also showed a moderate correlation; however, inclusion of both variables was likely to result in over-parameterization. We therefore selected vessel length and purse seine net length to represent vessel/gear characteristics contributing to efficiency changes. For the oceanographic metrics, thermocline depth, sea surface height, and depth of the 20° isotherm were highly correlated, while sea surface temperature, ENSO, and the variance in temperatures from the upper 200 m of the water column were all positively correlated. We selected thermocline depth to explain variability in catchability due to compression of the upper mixed layer, and ENSO to capture broad-scale fluctuations in sea surface temperature and the location of the convergence zone between the eastern and western waters. The salinity variables appeared to group by themselves; however, there were reasonably strong positive and negative correlations with the variables considered for inclusion, and therefore, salinity metrics not included in the model evaluations.

Figures 5 and 6 illustrate the distribution of the covariates, selected for inclusion in the candidate model suite, along with the observed relationship between yellowfin catch rates (mt/set). Nonlinearities between net length and thermocline depth and yellowfin catch rates were identified through exploratory analysis, therefore, we modeled these terms as splines in the candidate model set.

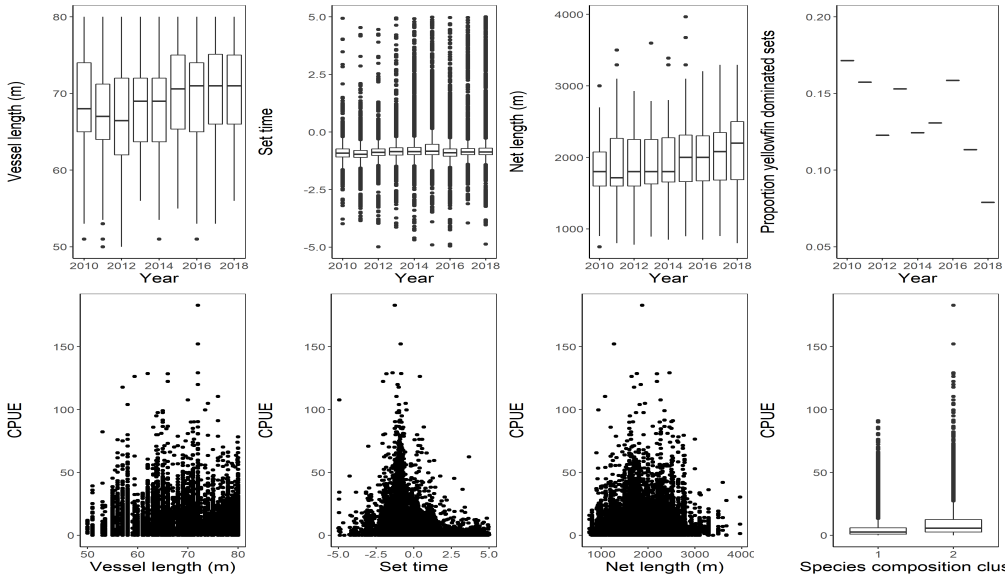

Figure 5: Distribution of covariate values (top), evaluated in the CPUE models, representing vessel, gear, and fishing strategy characteristics, from the filtered data set. On the bottom, yellowfin CPUE (mt/set) is plotted against the same covariates. The points represent individual observations from 2010-2018.

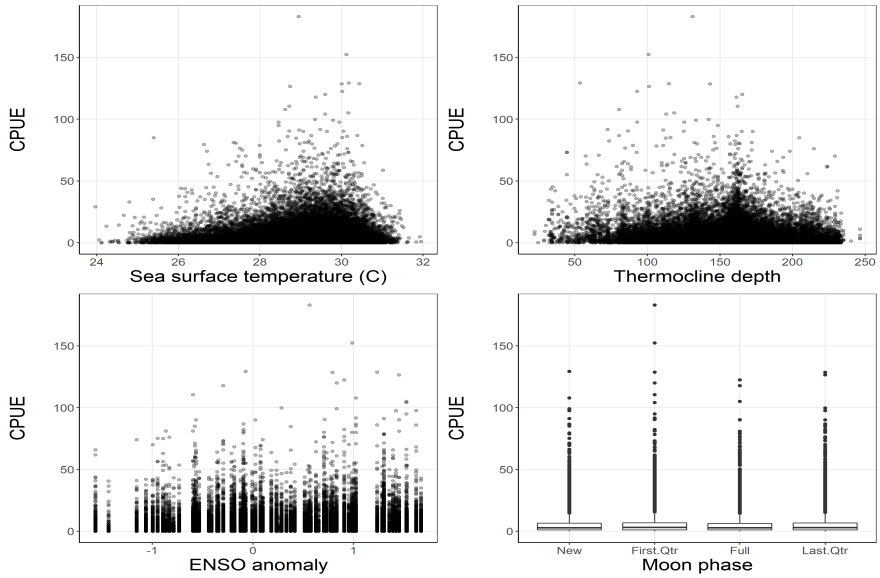

Figure 6: Distribution of environmental covariate values (top) evaluated in the CPUE models, and yellowfin CPUE (mt/set) plotted against the covariates (bottom), from the filtered data set. The points represent individual observations from 2010-2018.

2.3 Modeling approach

A suite of geostatistical delta generalized linear mixed models were implemented, using the *VAST* package in R (Thorson et al., 2015b), and were used to model yellowfin catch rates. Geostatistical models explicitly account for spatial and temporal autocorrelation in catch rates using smooth functions (Thorson et al., 2015b), addressing one of the potential pitfalls of traditional delta-GLMs. Each model component is estimated using Gaussian Markov random fields, assuming geometric anisotropy (i.e. the degree of spatial autocorrelation can vary based on directionality of neighboring knots) to allow for density predictions based on aggregate impacts of the environment and biological factors; factors that may influence the distribution of a given species as well as the catchability (Thorson, 2019b).

Quarterly yellowfin catch rates (mt/set) were modeled from 2010-2018, excluding the annual 3-month FAD closure period (July-September), using a delta-gamma spatiotemporal modeling framework. The probability of a positive catch was assumed to have a binomial error distribution, while we assumed a gamma error distribution for the magnitude of positive catches, as it has been shown to outperform the lognormal distribution when the underlying error distribution is misspecified (pers. comm J. Thorson). Specifically, the linear predictors for encounter probability and magnitude of positive catch rates (model component, encounter probability or positive catch rate, is denoted as m) are modeled for knot s and time step t, with the respective link functions (i.e., logit for the encounter probability and log link for the positive catch rates), as

$$m_i = \beta_m(t_i) + \eta_m(v_i) + \omega_m(s_i) + \epsilon_m(s_i, t) + \sum_{k=1}^{\eta_k} \lambda_k Q(i,k)$$

where β is the year-quarter effect, $\eta(v_i)$ is a random vessel effect, $\omega(s_i)$ is the spatial effect, $\epsilon(s_i, t)$ is the spatio-temporal effect, and λ_k represents the fixed catchability effects for $Q(i, k)$ catchability covariates. The spatial variation terms $\omega(s_i)$ were assumed to come from a Gaussian random field, and treated as random effects, assuming a Matern covariance matrix to account for spatial autocorrelation.

$$\omega_m \sim \text{MVN}(0, \sigma^2_{\omega m}\mathbf{R_m})$$

Separate decorrelation rates $\mathbf{R_m}$ (related to the anisotropy) were estimated for each model component (Thorson, 2019a). The spatio-temporal random effects $\epsilon(s_i, t)$ account for the interaction between time and the model spatial structure.

A random vessel effect was included to account for overdispersion and is assumed to follow a Gaussian distribution with a mean of zero and estimated variance parameter. Density at each knot in each time period $d(s, t)$ was estimated by obtaining the product of the back-transformed linear predictors, after dropping the catchability terms. The abundance index $I(t)$ at time t was then calculated as the sum of the area-weighted densities

$$I(t) = \sum_{s=1}^{N_s} a(s)d(s, t)$$

where $a(s)$ is the area associated with knot s. Regional indices were calculated as the area in each region associated with each knot, multiplied by the respective density; standard errors associated with the indices are calculated internally in Template Model Builder (TMB) using the inverse Hessian and the delta method (Thorson et al., 2016). The regional indices were estimated in terms of abundance; these estimates were then standardized to the mean to provide relative abundance trends over time.

2.3.1 Covariates

The catchability covariates $Q(i, k)$ evaluated included vessel length, net length, set time (hour before sunrise), species composition cluster, moon phase, and thermocline depth. Exploratory analyses indicated a non-linear relationships between catch rates and set time, thermocline depth, and net length, and therefore we evaluated the use of a zero-mean-constrained spline (Wood, 2015) to model these effects, such that the spline did not influence the model intercept (i.e. the year-quarter effect; Figure A.2).

Lastly, we evaluated the incorporation of a spatially-varying coefficient (SVC) to explain spatial variation in catch rates associated with ENSO (Thorson and Haltuch, 2019). During El Niño conditions the convergence zone between the western warm pool and the cooler eastern waters is pushed farther to the east, while in La Niña phases, the convergence zone is more to the west. As a result, the direction and magnitude of the effect of the ENSO phase on yellowfin density throughout the spatial domain of interest, may be highly variable. To address this source of variability, instead of estimating a single slope parameter associated with the ENSO covariate, SVCs were used to estimate a zero-centered spatially varying offset. The SVC is treated as a

random effect to estimate separate slopes for every modeled location, thereby allowing a range of density responses across space, to fluctuations in the ENSO index (Thorson, 2019c).

2.3.2 Spatial knots

Spatial locations at which the effects were estimated (i.e. the knots) were uniformly placed across the spatial domain with a specified number of knots (Figure 7). There is a tradeoff between the spatial resolution of the knot structure and model run time. Each additional knot adds parameters to the models on the order of the number of time steps multiplied by the number of model components (here, 2 components: encounter probability and magnitude of positive catches). We selected a knot value of 150, which approximates to a knot for every 2.5° x 2.5° cell in the extrapolation grid. The current version of *VAST* has the capability to perform bi-linear interpolation of abundance between knots. This interpolation tool is reasonably fast, and can provide improvements in the estimation in lieu of increasing the number of spatial knots. Observed data points were assigned to the nearest knot for estimation (Figure 7).

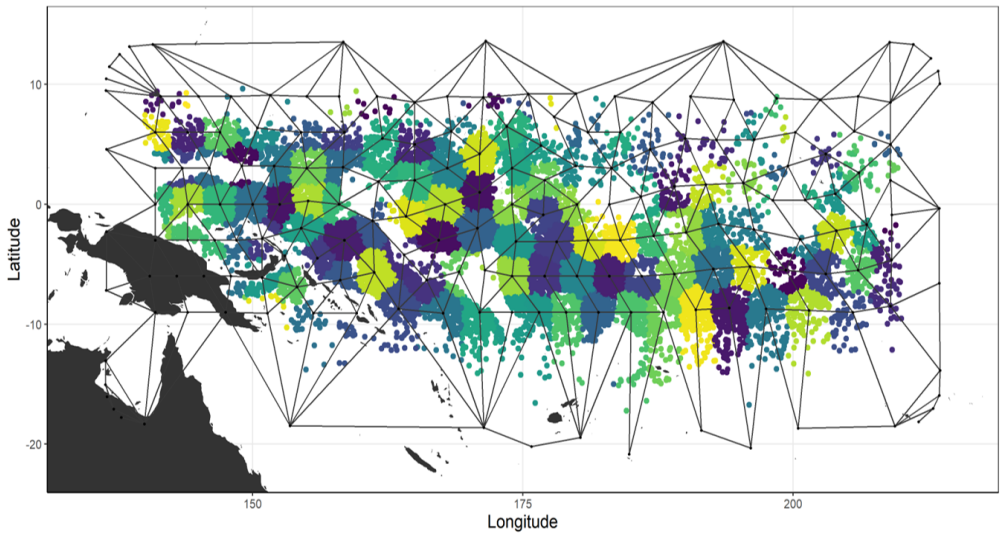

Figure 7: Spatial knot placement (uniform) and mesh configuration used in the geostatistical estimation model. Observation-level data points are color-coded based on the nearest knot.

2.4 Model diagnostics and selection

Competing models were evaluated using model convergence statistics, Akaike's Information Criterion (AIC), assessing coefficient estimates for variable selection, and comparison of similar models with the interest in adopting the simplest model when multiple models were providing similar results. Model diagnostics were employed to evaluate model fit and potential violation of model assumptions, including evaluation of distributional assumptions, influence measures

(Bentley et al., 2012), and analysis of residuals. For comparison, the estimated mean-standardized recruitment indices from the competing models were compared to each other, as well as to the nominal CPUE.

2.5 Fishing efficiency

Changes in fishing efficiency under an effort-based management scheme, is often referred to as effort creep (Pilling et al., 2016). Failing to account for effort creep can lead lead to incorrect interpretations of trends in abundance due to potentially hyperstable catch rates. Hyperstability refers to the situation where catch rates remain high even as the underlying abundance declines (Harley et al., 2001). This an important concern for industrial fisheries generally, but specifically for the tuna purse seine fisheries. Technology and use of FADs has rapidly enhanced the sophistication of knowledge fishers have access to, and as a result, they may be better equipped to locate and harvest tuna schools more efficiently, thereby maintaining catch rate levels while abundance declines.

Quantifying efficiency gains and appropriately mapping those changes to fluctuations in fishing mortality or catch rates is often difficult. Global estimates of effort creep generally range between 2 - 5% per annum (Palomares and Pauly, 2019). We have yet to develop a reliable, data-driven metric of effort creep from the dFAD fishery, suitable for use as an effort adjustment; however, work is ongoing to address this important knowledge gap. In the absence of such a metric, we have applied a 2% and 5% effort correction pd, per annum, to evaluate potential changes in the abundance index as a result. Following Palomares and Pauly (2019), the annual correction factor Corr_t, where t represents years from $t = 0$ (i.e. 2010), will then be applied to the adjust the estimated index values, in each year.

$$\text{Corr}_t = (1 - pd)^t$$

$$\text{CPUE}_{\text{Corr}_t} = \text{CPUE}_t \cdot \text{Corr}_t$$

3 Results

The nominal CPUE indices have been fairly stable through time (Figure 8), with a slight decline in Region 4 over the time series, while Regions 3 and 8 demonstrated modest increases between 2015 and 2017.

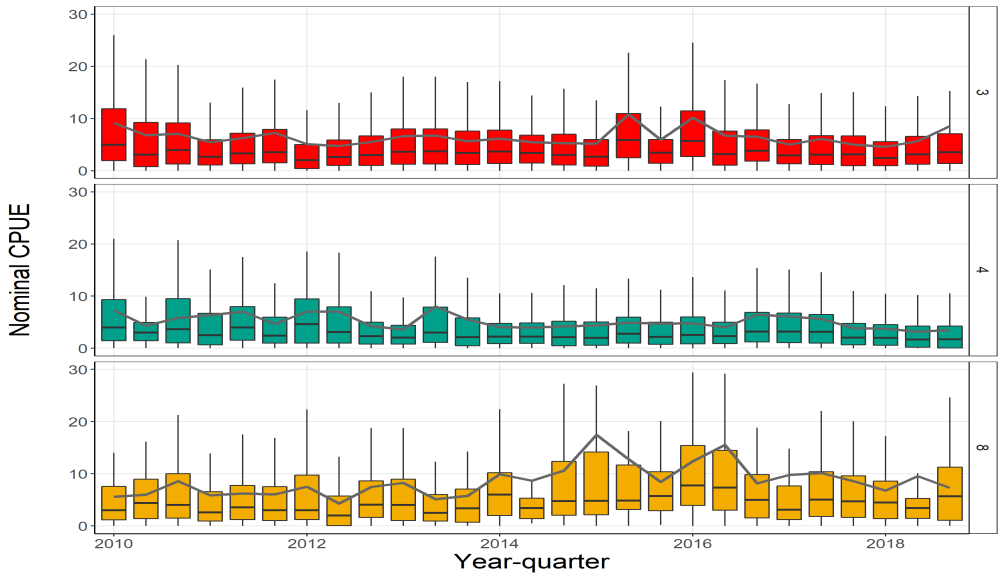

Figure 8: Distribution of nominal yellowfin CPUE (mt/set) in the three Regions of interest (3, 4, and 8) with the gray line representing the mean nominal CPUE (mt/set).

There was little contrast between the resulting abundance indices estimated from the competing models (Figure 9); however, we selected a 'preferred' model (i.e. Model 5) based on model selection criteria and an interest in retaining the simplest model from those deemed indistinguishable based on the information criterion (Table 4).

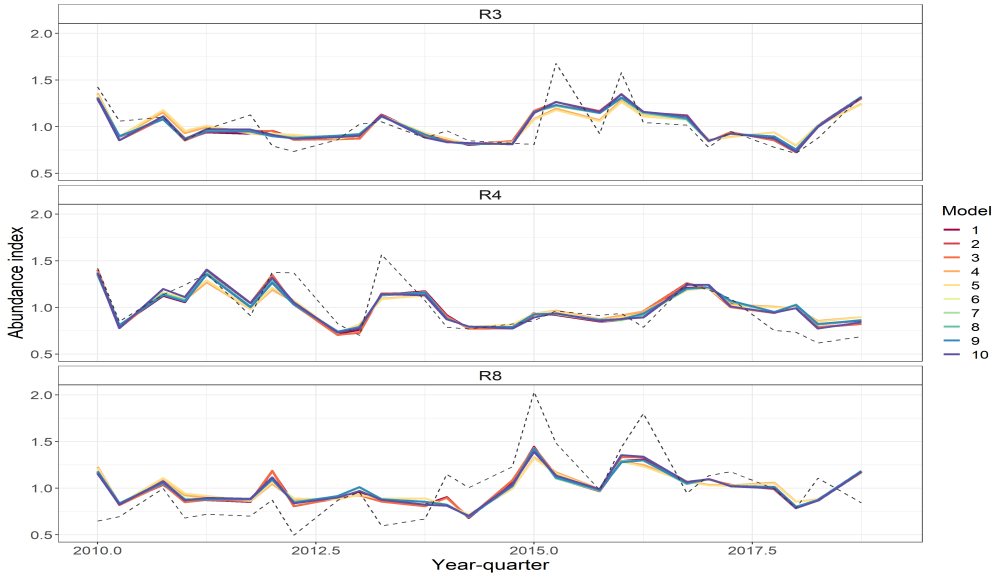

Figure 9: Comparison of relative abundance indices from competing models alongside the mean-standardized nominal CPUE, separated by assessment region, from 2010-2018.

Model	Covariates	AIC	Δ AIC
1	CL + MP + VL + s(ST) + s(NL) + s(TD) + svc(ENSO)	213735.8	7175.4
2	MP + VL + s(ST) + s(NL) + s(TD) + svc(ENSO)	213742.3	7181.9
3	MP + VL + s(ST) + s(TD) + svc(ENSO)	207896.0	1335.6
4	CL + VL + s(ST) + s(NL) + s(TD) + svc(ENSO)	206563.3	2.9
5	**CL + VL + s(ST) + svc(ENSO)**	206560.4	0
6	VL + s(ST) + s(NL) + s(TD) + svc(ENSO)	207913.8	1353.4
7	VL + s(ST) + s(NL)+ svc(ENSO)	207905.5	1345.1
8	VL + s(ST) + svc(ENSO)	207912.8	1352.4
9	CL + s(ST) + svc(ENSO)	206566.5	6.1
10		208048	1487.6

Table 4: Suite of model configurations evaluated, with corresponding AIC values used for model selection. Covariates are indicated by the following: MP = moon phase; CL = species composition cluster; VL = vessel length; ST = set time (hours before sunrise); NL = net length; TD = thermocline depth; ENSO = El Niño Southern Oscillation index; and SST = sea surface temperature. An s() around the covariate abbreviation indicates it was fitted as a spline, while svc() indicates a spatially varying coefficient. Model 5, in bold font, was identified as the preferred model.

The preferred model included the species composition variable, vessel length, set time (hours before sunrise), with ENSO as a spatially varying density covariate. The three regions had similar trends in abundance through time, with Region 4 (the easternmost region) exhibiting the greatest variability. Overall, abundance trends were fairly stable throughout the time period (Figures 10 and 11). Regions 3 and 8 both had a brief period of increased abundance from approximately 2015-2016, followed by a modest decline through 2017. In Region 4, the biomass estimates were consistently higher than the other regions, but also more variable, with ephemeral spikes in the index throughout the time series.

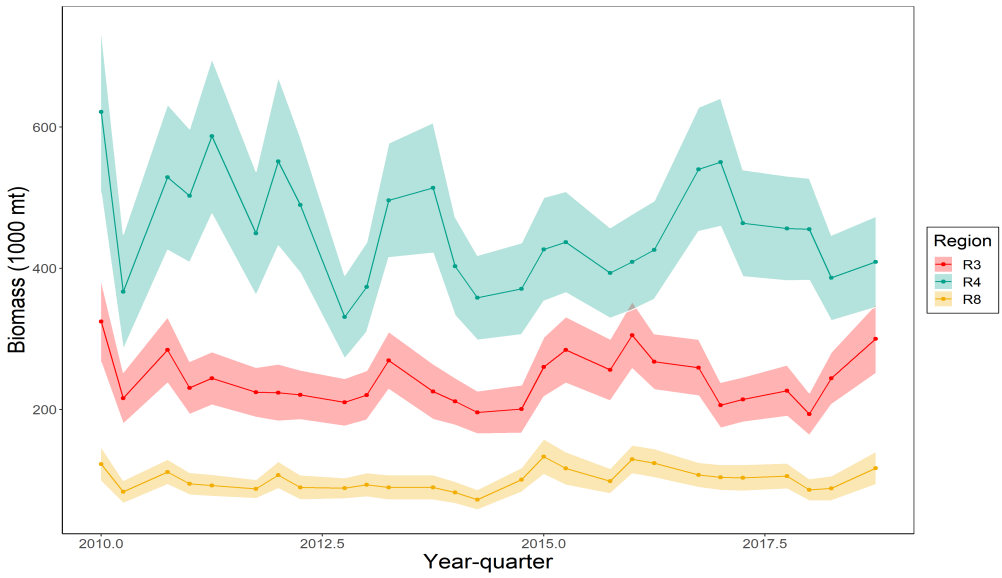

Figure 10: Area-weighted biomass estimates (1000 mt) for Regions 3, 4, and 8 of the 2017 yellowfin tuna stock assessment.

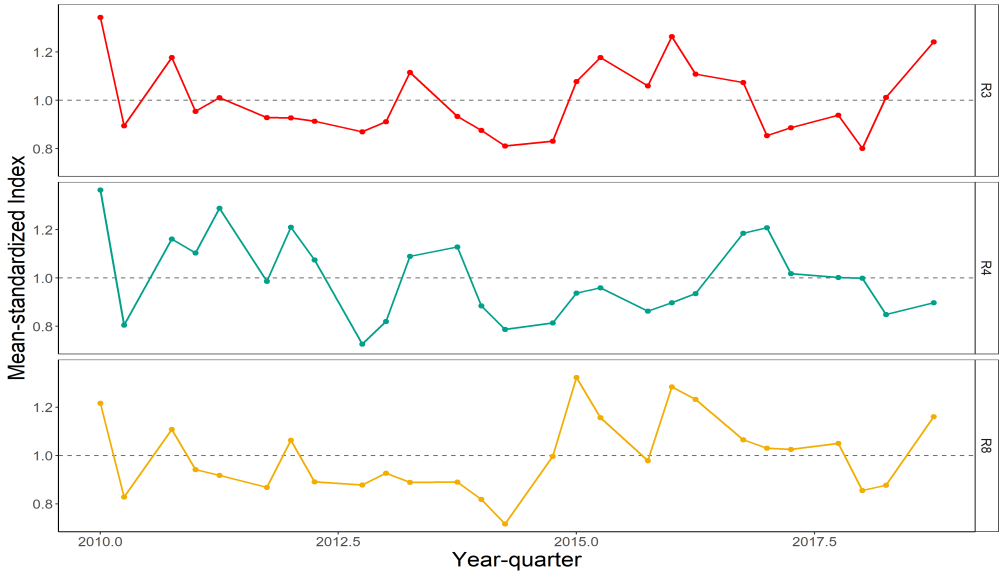

Figure 11: Mean-standardized index estimates (solid lines with points) for Regions 3, 4, and 8 of the 2017 yellowfin tuna stock assessment, with the gray dashed line representing the standardized time series mean.

The catchability covariates were predicted to explain a combination of fisher and tuna behavior. The species composition cluster suggested, naturally, that the 'yellowfin' cluster (cluster 2) produced higher yellowfin catch rates. This variable was included to control for the multi-species aspect of this fishery and for the fact that fishers do not often know the species composition of the school prior to setting the net. Vessel length, although restricted to the 50-80 m size range,

remained an important covariate, although with a modest effect. The majority of the vessels participating in the purse seine fishery fall within the 50-80 m range, but even so, there has been a gradual increase in vessel size within this size class (Vidal et al., 2019). Set time was included in the model to capture variability in catch rates associated with the diurnal tuna behavior. The main distribution of set times spanned from approximately three hours before to two hours after sunrise, with the peak just before the sun rises over the horizon. We included sets that spanned +/- five hours from sunrise, thereby excluding afternoon sets. Catch rates were generally highest pre-dawn, and declined into the morning hours. The inclusion of the ENSO effect suggested a better fit to the data, although the spatial variability was relatively small (σ = 0.1). Across the entire spatial domain there was generally little contrast in the effect of ENSO; however, this variable is capturing variability in the regions where ENSO phase shifts have important effects on habitat, and therefore, it was retained as a spatially-varying covariate.

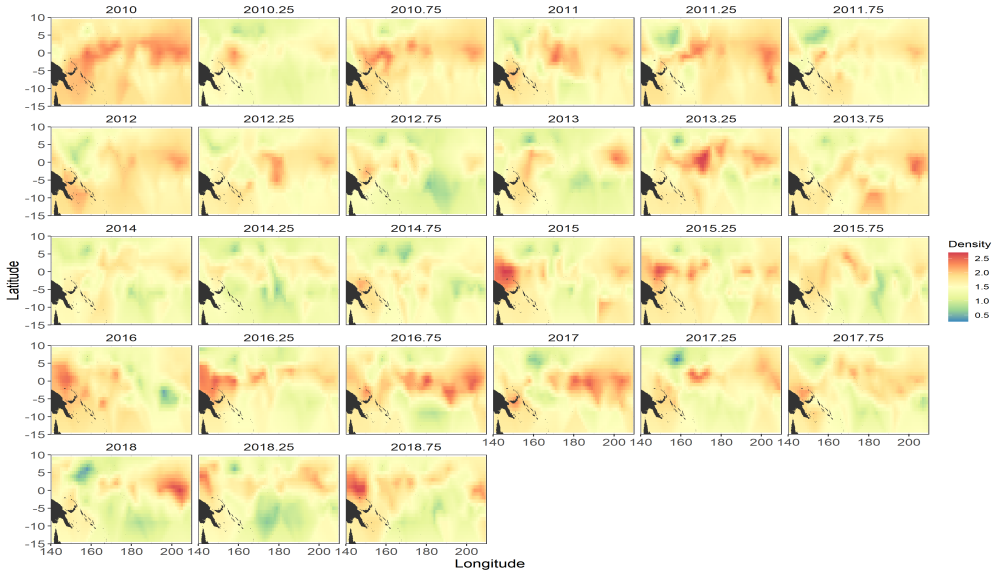

Figure 12: Predicted density (log mt/km^2) throughout the spatial domain for the time series, 2010-2018.

Model diagnostics did not suggest any major issues for the model fit. The q-q plot (Figure A.3) demonstrated reasonable adherence to the 1:1 line, without systematic or large departures, suggesting reasonable assumptions with respect to the error distributions. The distribution of mean residuals across the extrapolation grid, for both the encounter probability (Figure A.4) and the positive catch rate (Figure A.5) components, suggested a random distribution of positive and negative residuals, without any strong patterning through time. In addition, no strong trends in the influence measures were detected for the covariates included (Figure A.3).

We have yet to develop a reliable metric of effort creep, and given the potential impact efficiency changes might have on the index over time (e.g. leading to hyperstability), we have implemented general effort adjustments of 2 and 5% for reference. The departures from the estimated index increase through time (Figure 13), but the 2% effort adjustment results in indices which are

contained within the confidence intervals for the estimated indices; however the 5% adjustment falls below the lower confidence bounds for the most recent years.

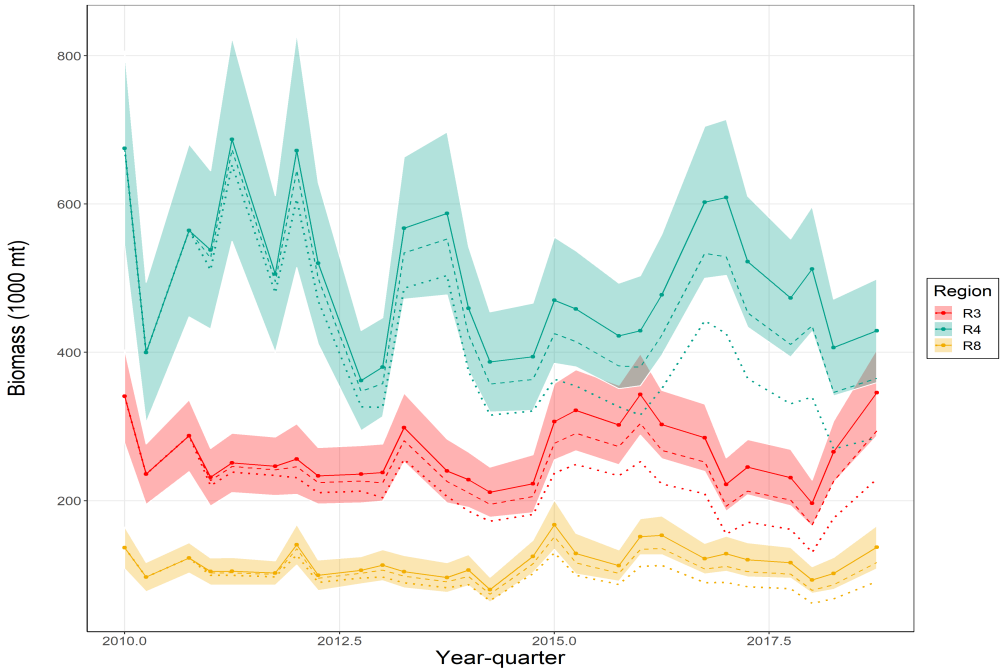

Figure 13: Illustration of the influence a 2 and 5% per annum increase in effective effort was predicted to have on the estimated abundance indices.

4 Discussion

Understanding recruitment dynamics for yellowfin is important to inform the stock assessment model as well as for general surveillance of the population. In the WCPO, direct estimates of yellowfin recruitment are lacking, and therefore, recruitment has traditionally been estimated internally by the stock assessment models (Tremblay-Boyer et al., 2017). Here, we have presented a CPUE standardization model for the juvenile component of the fishery to better inform the model on the recruitment process. The index alone may not directly address recruitment due to the potential mixture of age classes in the catches; however the index will be evaluated in concert with gear specific selectivities and size-composition data to disentangle the juvenile signal from the entirety of the catches to produce recruitment estimates.

Using observer collected data from a time period with 100% coverage enabled an analysis with comprehensive data on purse seine activity in the region. The estimated abundance indices were relatively stable over the time series evaluated, in contrast to the recruitment estimates from the last assessment, which showed high inter-annual variability, especially in Region 3. The estimated standardized trends are plausible, as biomass was estimated to be fairly stable between 2010 and 2015 (Tremblay-Boyer et al., 2017); however the presence of multiple cohorts in the catches could

smooth through some of the variability associated with individual recruitment events. Spawning behavior of yellowfin further complicates recruitment estimation because they do not adhere to a discrete spawning season, but instead have been found actively spawning throughout the year, when conditions are favorable (Itano, 2000; Sun et al., 2005). Therefore, identifying discrete cohorts remains a challenge.

For this analysis, we developed and evaluated a suite of variables predicted to influence yellowfin catch rates to include in the standardization models, and yet, most were not highly influential. However, we suspect that the flexibility of the model to implicitly capture variation in space and time is explaining some of the variability that might otherwise be explicitly explained by the covariates (e.g. Hodges and Reich, 2010). Of course, there is the potential for influential, but unknown (either unidentified or identified by lacking adequate data), factors to be informing fisher decision-making processes and ultimately catch rates. Fishing technologies and strategies are continually evolving to improve efficiency and maximize profits, and as a result, fishers are theoretically able to make more informed decisions about where and when to fish. Improving our understanding of these decision points is paramount for analyzing and interpreting CPUE.

Oceanographic conditions throughout the equatorial region tend to be fairly homogeneous compared to the more temperate regions of the Pacific. Even so, there are important complexities associated with the regional currents and countercurrents, and interactions with broad climatic phenomena (e.g. Yen et al., 2017). Demographic processes in marine fishes can be strongly influenced by environmental variability at various life stages from egg through the adult phase, especially at the limits of a species' geographic range (Myers, 1998). Because we do not have reliable information on earlier life stages, we have used recruitment to the fishery (approximately age-1) to develop a recruitment index. Therefore, fluctuations in the index reflect the combined mortality from various earlier life stages. The environmental covariates included here were largely to account for changes in catchability (i.e. thermocline depth) and relative density at the time of the fishing activity (i.e. ENSO), but further work to better understand the mechanisms underlying recruitment success from hatch to capture in the fishery is needed.

Given the magnitude of the purse seine fishery, catch and effort data are likely to contain valuable information regarding recruitment trends for yellowfin tuna; however, catch trends may not be able to tell the whole story. To buffer against uncertainty, we recommend the development of complementary approaches to better capture trends in recruitment variability. Specifically, prioritizing validation of an aging method for yellowfin to build confidence in the age composition estimates in the WCPO and to enable production aging to shed light on changes in the age structure of the population over time. It may also be possible to develop recruitment proxies from diet analyses; data for which are readily available from work done by the Pacific Community (SPC). In addition, future work could focus on incorporating multiple data sources to further validate the signals detected from the CPUE analysis. For example, matching cohorts from longline and purse seine catches (using length frequency data) and further exploring correlation between the two as well as their relationships with CPUE and variability in the environment.

Lastly, we recognize the role effort creep plays in the purse seine fishery, and specifically the impacts associated with drifting FADs, cannot be ignored. Hyperstability is one of the main

concerns with using purse seine catch and effort to inform the assessment process, and here, a hyperstable CPUE index could mask variability in abundance associated with strong cohorts, thereby dampening the signal of interest. This analysis has not explicitly addressed effort creep, but doing so remains a top priority moving forward. There is ongoing work to develop a fisher survey to better understand changes in fishing strategy and efficiency through time, to quantify the influence of these changes on catch rates, and address factors influencing the decision making processes (see Wichman et al., 2020). In addition, we are exploring the impacts of FAD density and FAD technologies on catch rates. Advancing our understanding of changes in fishing mortality over time is paramount for the reliability of purse seine based abundance indices. Here, we have demonstrated an approach, using purse seine dFAD catch and effort information, to characterize recruitment trends in yellowfin, but the intention is to extend this modeling framework to better characterize skipjack abundance trends as well (Vidal et al., 2020a).

5 Acknowledgements

We thank the Pacific-European Union Marine Partnership (PEUMP) Programme for funding TV's position, under KRA 1.5 'Improved modelling of relative abundance using catch per unit effort', which has facilitated these analyses, and Jim Thorson et al. for the development of the VAST package as well as for hosting workshops to help participants understand the modeling tool better and utilize it more effectively. We also thank Elizabeth Heagney for valuable comments on an earlier draft and the participants of the ePAW for constructive feedback on the analysis.

6 References

Agafonkin, V. and Thieurmel, B. (2017). suncalc: Compute sun position, sunlight phases, moon position, and lunar phase. R package version 0.3.

Arrizabalaga, H., Dufour, F., Kell, L., Merino, G., Ibaibarriaga, L., Chust, G., Irigoien, X., Santiago, J., Murua, H., Fraile, I., et al. (2015). Global habitat preferences of commercially valuable tuna. *Deep Sea Research Part II: Topical Studies in Oceanography*, 113:102–112.

Banzon, V., Reynolds, R., and National Center for Atmospheric Research Staff (Eds) (2019). The Climate Data Guide: SST data: NOAA High-resolution (0.25x0.25) Blended Analysis of Daily SST and Ice, OISSTv2. https://climatedataguide.ucar.edu/climate-data/sst-data-noaa-high-resolution-025x025-blended-analysis-daily-sst-and-ice-oisstv2. Accessed: 2019-10-10.

Bentley, N., Kendrick, T. H., Starr, P. J., and Breen, P. A. (2012). Influence plots and metrics: tools for better understanding fisheries catch-per-unit-effort standardizations. *ICES Journal of Marine Science*, 69(1):84–88.

Bigelow, K. A., Boggs, C. H., and He, X. (1999). Environmental effects on swordfish and blue shark catch rates in the US North Pacific longline fishery. *Fisheries Oceanography*, 8(3):178–198.

Bigelow, K. A. and Maunder, M. N. (2007). Does habitat or depth influence catch rates of pelagic species? *Canadian Journal of Fisheries and Aquatic Sciences*, 64(11):1581–1594.

Dunn, S., Rodwell, L., and Joseph, G. (2006). The Palau Arrangement for the management of the Western Pacific purse seine fishery-management scheme (Vessel Day Scheme). In *Sharing the Fish Conference, Perth*.

Evans, K., Langley, A., Clear, N. P., Williams, P., Patterson, T., Sibert, J., Hampton, J., and Gunn, J. S. (2008). Behaviour and habitat preferences of bigeye tuna (*Thunnus obesus*) and their influence on longline fishery catches in the western Coral Sea. *Canadian Journal of Fisheries and Aquatic Sciences*, 65(11):2427–2443.

Fiedler, P. C. and Bernard, H. J. (1987). Tuna aggregation and feeding near fronts observed in satellite imagery. *Continental shelf research*, 7(8):871–881.

Harley, S., Williams, P., and Hampton, J. (2009). Analysis of purse seine set times for different school associations: a further tool to assist in compliance with FAD closures? *Western and Central Pacific Fisheries Commission 5th Regular Session*, WCPFC-SC5-2009/ ST-WP-07, Port Vila, Vanuatu.

Harley, S. J., Myers, R. A., and Dunn, A. (2001). Is catch-per-unit-effort proportional to abundance? *Canadian Journal of Fisheries and Aquatic Sciences*, 58(9):1760–1772.

Hodges, J. S. and Reich, B. J. (2010). Adding spatially-correlated errors can mess up the fixed effect you love. *The American Statistician*, 64(4):325–334.

Howell, E. A. and Kobayashi, D. R. (2006). El Niño effects in the Palmyra Atoll region: oceanographic changes and bigeye tuna (*Thunnus obesus*) catch rate variability. *Fisheries Oceanography*, 15(6):477–489.

Itano, D. G. (2000). *The reproductive biology of yellowfin tuna (Thunnus albacares) in Hawaiian waters and the western tropical Pacific Ocean: project summary*. University of Hawaii, Joint Institute for Marine and Atmospheric Research Hawaii.

Langley, A., Briand, K., Kirby, D. S., and Murtugudde, R. (2009). Influence of oceanographic variability on recruitment of yellowfin tuna (*Thunnus albacares*) in the western and central Pacific Ocean. *Canadian Journal of Fisheries and Aquatic Sciences*, 66(9):1462–1477.

Lehodey, P., Bertignac, M., Hampton, J., Lewis, A., and Picaut, J. (1997). El Niño Southern Oscillation and tuna in the western Pacific. *Nature*, 389(6652):715–718.

Lowry, M., Williams, D., and Metti, Y. (2007). Lunar landings–Relationship between lunar phase and catch rates for an Australian gamefish-tournament fishery. *Fisheries Research*, 88(1-3):15–23.

Lumban-Gaol, J., Leben, R. R., Vignudelli, S., Mahapatra, K., Okada, Y., Nababan, B., Mei-Ling, M., Amri, K., Arhatin, R. E., and Syahdan, M. (2015). Variability of satellite-derived sea surface height anomaly, and its relationship with Bigeye tuna (*Thunnus obesus*) catch in the Eastern Indian Ocean. *European Journal of Remote Sensing*, 48(1):465–477.

Myers, R. A. (1998). When do environment–recruitment correlations work? *Reviews in Fish Biology and Fisheries*, 8(3):285–305.

Palomares, M. and Pauly, D. (2019). On the creeping increase of vessels' fishing power. *Ecology and Society*, 24(3).

Parties to the Nauru Agreement (2016). Palau Arrangement for the management of the Western Pacific fishery as amended - management scheme (purse seine Vessel Day Scheme). Technical report.

Pilling, G., Tidd, A., the PNA Office, Norris, W., and Hampton, J. (2016). Examining indicators of effort creep in the WCPO purse seine fishery. *Western and Central Pacific Fisheries Commission 12th Regular Session*, WCPFC-SC12-2016/MI-WP-08.

Royer, F., Fromentin, J.-M., and Gaspar, P. (2004). Association between bluefin tuna schools and oceanic features in the western Mediterranean. *Marine Ecology Progress Series*, 269:249–263.

Sun, C., Wang, W., and Su-Zan, Y. (2005). Reproductive biology of the female yellowfin tuna *Thunnus albacares* in the western Pacific Ocean. *WCPFC–SC1-2005/ BI WP–1*.

Thorson, J. T. (2019a). Forecast skill for predicting distribution shifts: a retrospective experiment for marine fishes in the Eastern Bering Sea. *Fish and Fisheries*, 20(1):159–173.

Thorson, J. T. (2019b). Guidance for decisions using the Vector Autoregressive Spatio-Temporal (VAST) package in stock, ecosystem, habitat and climate assessments. *Fisheries Research*, 210:143–161.

Thorson, J. T. (2019c). Measuring the impact of oceanographic indices on species distribution shifts: The spatially varying effect of cold-pool extent in the eastern Bering Sea. *Limnology and Oceanography*, 64(6):2632–2645.

Thorson, J. T. and Haltuch, M. A. (2019). Spatiotemporal analysis of compositional data: increased precision and improved workflow using model-based inputs to stock assessment. *Canadian Journal of Fisheries and Aquatic Sciences*, 76(3):401–414.

Thorson, J. T., Pinsky, M. L., and Ward, E. J. (2016). Model-based inference for estimating shifts in species distribution, area occupied and centre of gravity. *Methods in Ecology and Evolution*, 7(8):990–1002.

Thorson, J. T., Scheuerell, M. D., Shelton, A. O., See, K. E., Skaug, H. J., and Kristensen, K. (2015a). Spatial factor analysis: a new tool for estimating joint species distributions and correlations in species range. *Methods in Ecology and Evolution*, 6(6):627–637.

Thorson, J. T., Shelton, A. O., Ward, E. J., and Skaug, H. J. (2015b). Geostatistical delta-generalized linear mixed models improve precision for estimated abundance indices for west coast groundfishes. *ICES Journal of Marine Science: Journal du Conseil*, page fsu243.

Tremblay-Boyer, L., McKechnie, S., Pilling, G., and Hampton, J. (2017). Stock assessment of yellowfin tuna in the western and central Pacific Ocean. *Western and Central Pacific Fisheries Commission 13th Regular Session*, WCPFC-SC13-2017/ SA-WP-06.

Vidal, T., Hamer, P., Escalle, L., and Pilling, G. (2020a). Assessing trends in skipjack tuna abundance from purse seine catch and effort data in the WCPO. *Western and Central Pacific Fisheries Commission 16th Regular Session*, WCPFC-SC16-2020/ SA-IP-09.

Vidal, T., Hamer, P., Wichman, M., and the PNAO (2020b). Examaining indicators of technological and effort creep in the WCPO purse seine fishery. *Western and Central Pacific Fisheries Commission 16th Regular Session*, WCPFC-SC16-2020/ MI-IP-15.

Vidal, T., Muller, B., Pilling, G., and the PNAO (2019). Evaluation of effort creep indicators in the WCPO purse seine fishery. *Western and Central Pacific Fisheries Commission 15th Regular Session*, WCPFC-SC15-2019/ MI-IP-05.

Wichman, W., Vidal, T., and Hamer, P. (2020). Purse seine effort creep research plan. *Western and Central Pacific Fisheries Commission 16th Regular Session*, WCPFC-SC16-2020/ MI-IP-16.

Williams, P. and Reid, C. (2019). Overview of Tuna Fisheries in the Western and Central Pacific Ocean, including Economic Conditions – 2018. *Western and Central Pacific Fisheries Commission 15th Regular Session*.

Wood, S. (2015). Package 'mgcv'. *R package version*, 1:29.

Yen, K.-W., Wang, G., and Lu, H.-J. (2017). Evaluating habitat suitability and relative abundance of skipjack (*Katsuwonus pelamis*) in the Western and Central Pacific during various El Niño events. *Ocean & coastal management*, 139:153–160.

Young, J., Hobday, A., Campbell, R., Kloser, R., Bonham, P., Clementson, L., and Lansdell, M. (2011). The biological oceanography of the East Australian Current and surrounding waters in relation to tuna and billfish catches off eastern Australia. *Deep Sea Research Part II: Topical Studies in Oceanography*, 58(5):720–733.

Appendix

A.1 Supplemental figures

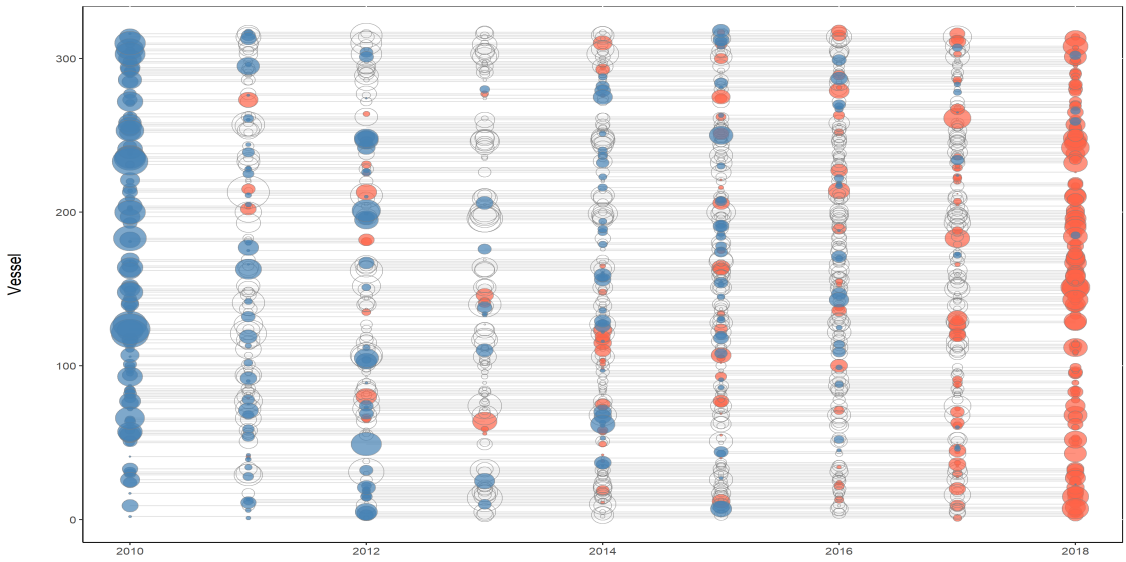

Figure A.1: Vessel participation history and relative contribution to annual catches. The blue symbols indicate when a vessel entered the fishery, and the red colored symbols indicate the most recent observation from that vessel. Each line on the y-axis represents a unique vessel. The symbol sizes are scaled by the individual vessel's relative contribution to total catches in each year.

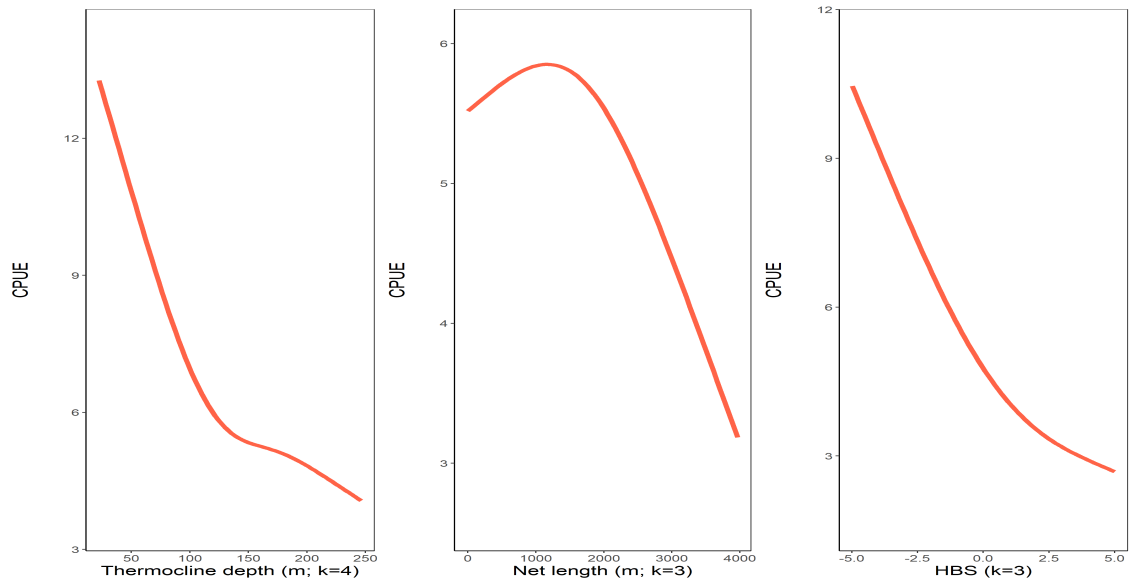

Figure A.2: Illustration of the nonlinear relationship between yellowfin CPUE and the catchability covariates (set time, net length, and thermocline depth), fitted using a zero-mean-constrained spline with k knots.

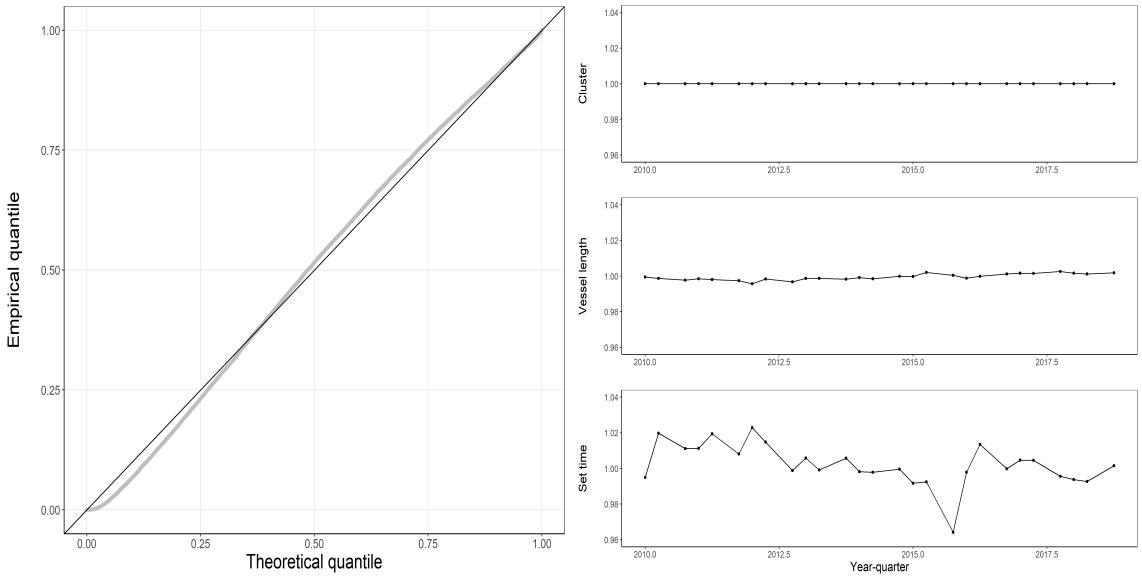

Figure A.3: Q-Q plot presented as a diagnostic measure of model fit for the positive catch component (left), and influence plots for the catchability covariates (right).

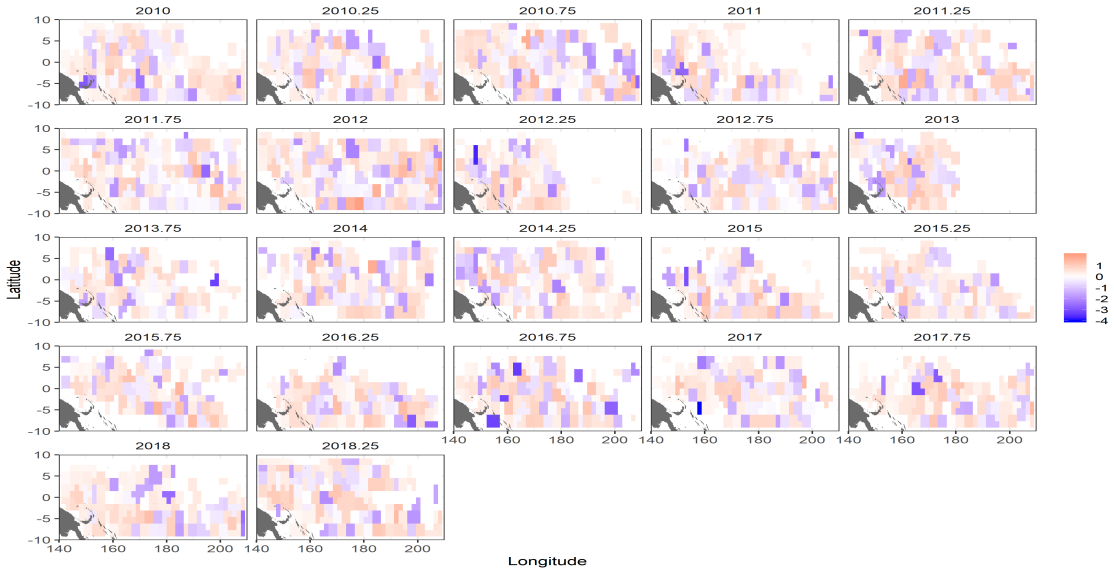

Figure A.4: Mean Pearson residuals for the encounter probability, by extrapolation grid cell.

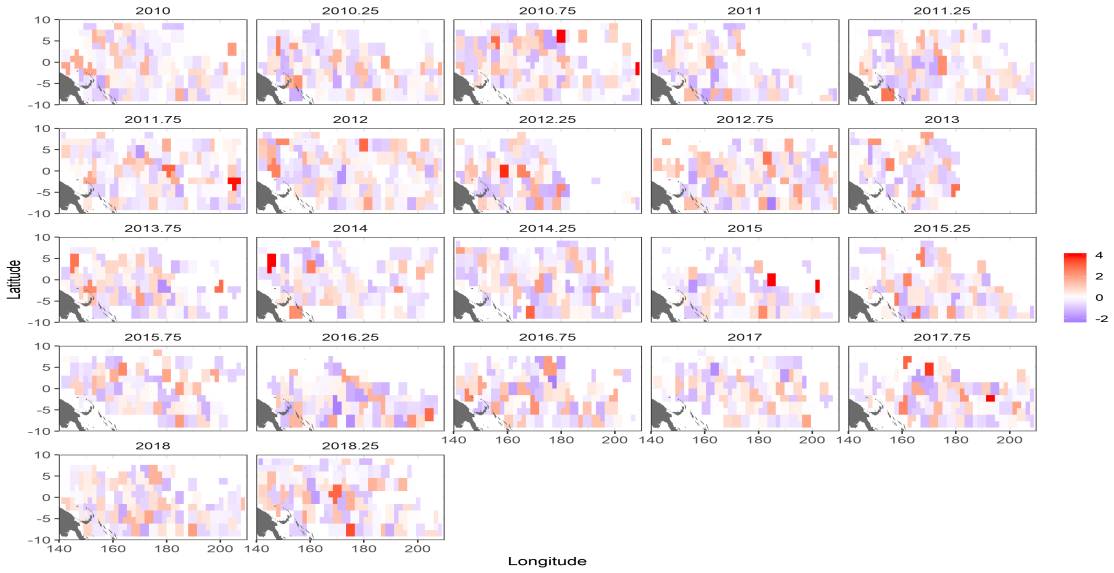

Figure A.5: Mean Pearson residuals for the positive catch rates, by extrapolation grid cell.

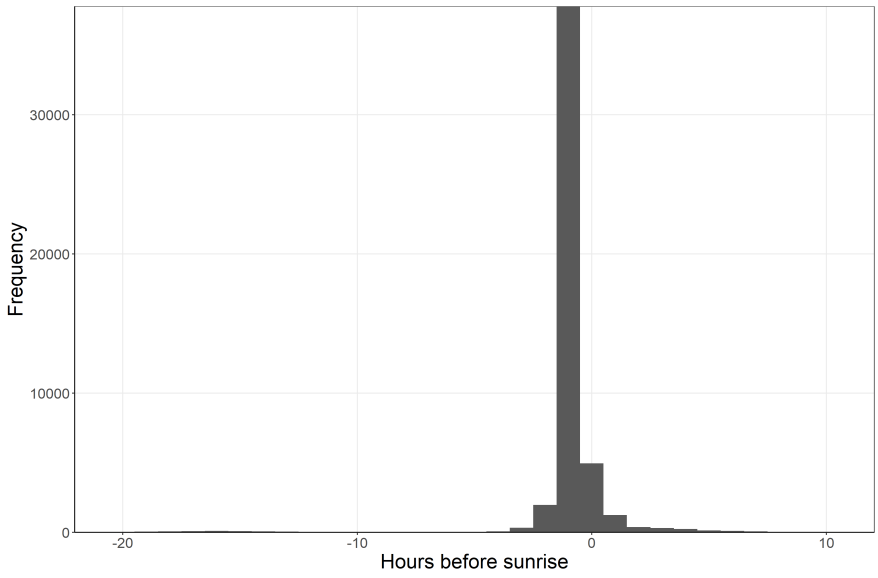

Figure A.6: Distribution of observer reported drifting FAD set times, relative to sunrise, prior to data filtering.

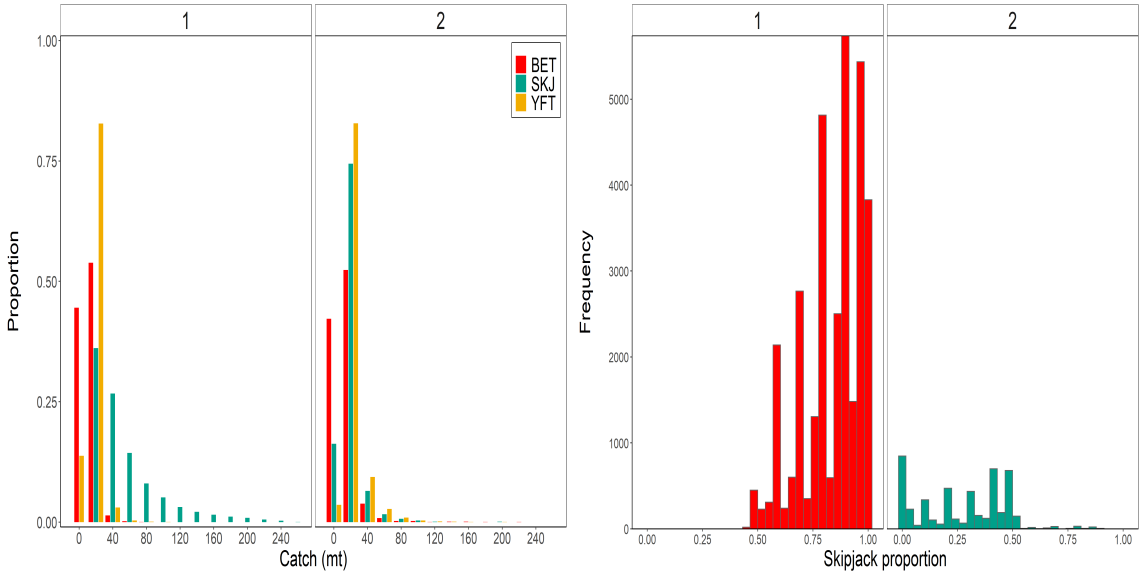

Figure A.7: Proportion of catch sizes, binned to 20 mt, associated with the three main tuna species for each of the two species composition clusters used in the models (left). On the right, is the observed frequency of the proportion of the dFAD set catches attributed to skipjack. These figures highlight the differences in catch composition captured by the clustering approach. Cluster 1 is therefore, the cluster that is dominated by skipjack tuna, whereas cluster 2 tends to have relatively higher proportions of yellowfin and bigeye.

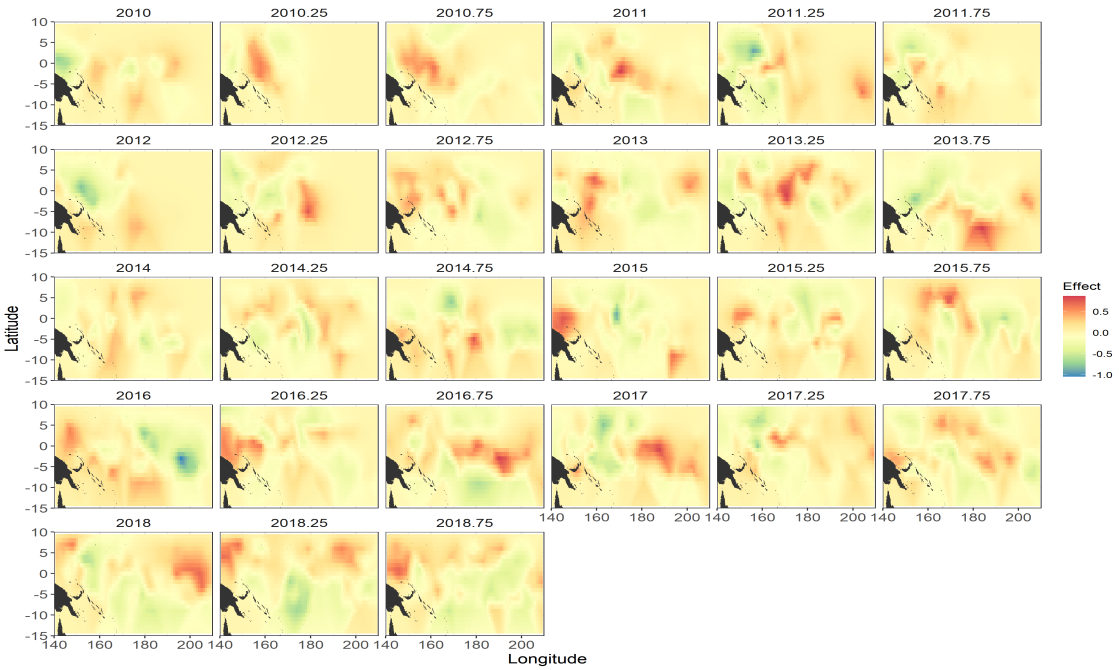

Figure A.8: Distribution of random spatio-temporal density effects, drawn from a Markov Gaussian random field with a mean of zero.

A.2 Logbook indices

For comparison, the logbook data were fitted with a similar model structure, to compare to the observer generated indices, but for a longer time series (2000-2018). The model included, lunar phase, vessel length, and nonlinear terms for set time and thermocline depth as catchability covariates, with a spatially varying coefficient for the ENSO effect on density.

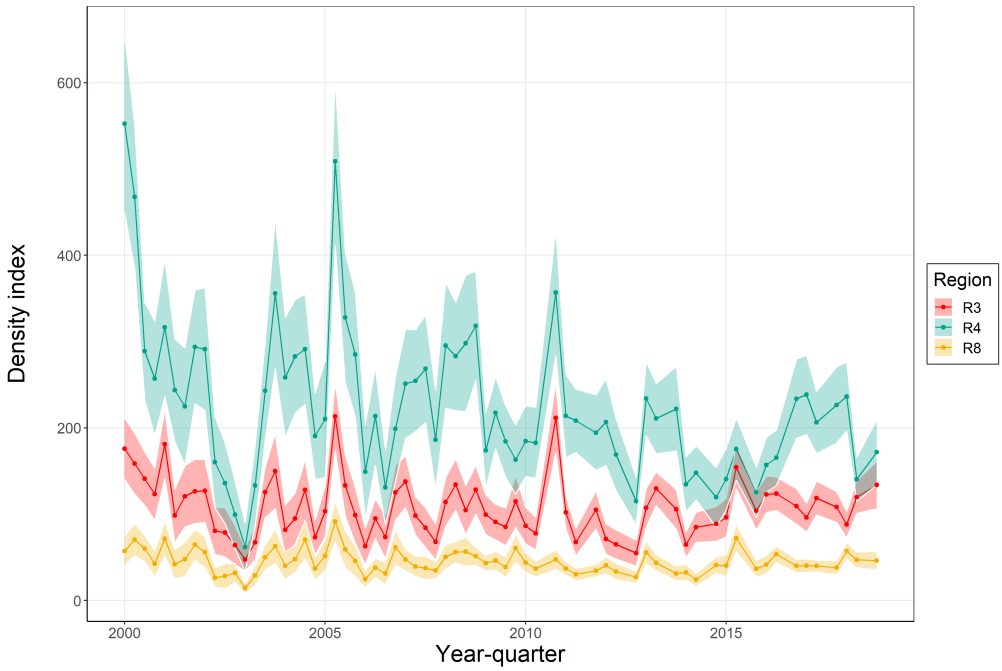

Figure A.9: Predicted abundance index using logbook data from 2000-2018. The model structure was similar, except that net length was unavailable and was therefore not included.

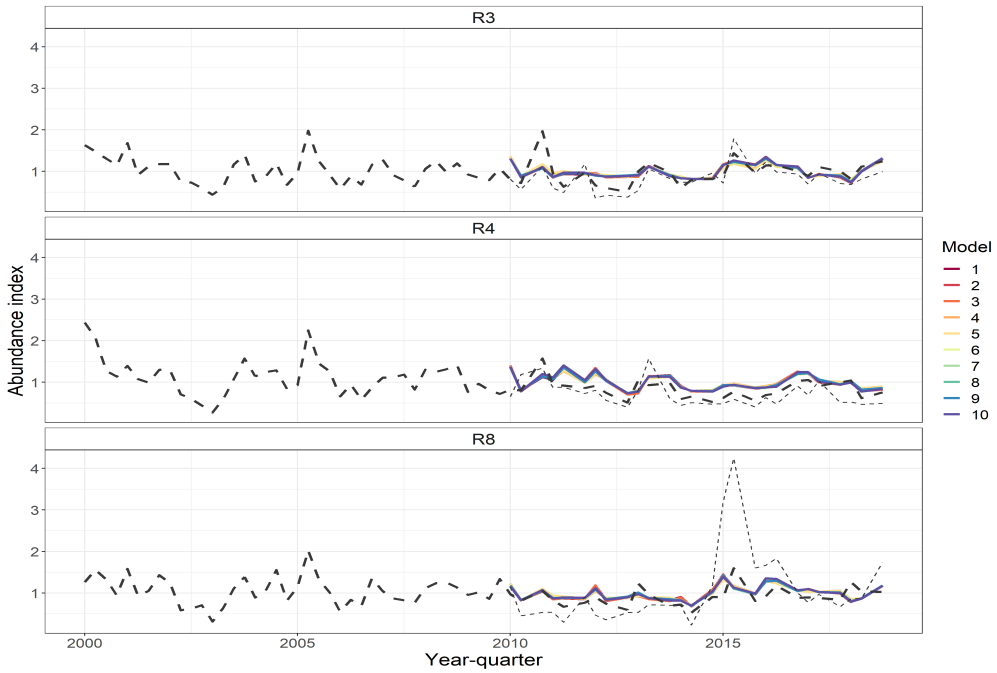

Figure A.10: Comparison of mean-standardized abundance indices from competing models estimated from observer data combined with the indices estimated from the same model, but using logsheet data (dark dashed line), separated by assessment region, from 2000-2018. The thin dashed line is the nominal CPUE (mean mt/set) from the observer data.